

PAPER

The nature of graphene–metal bonding probed by Raman spectroscopy: the special case of cobalt

To cite this article: Inés Serrano-Esparza *et al* 2016 *J. Phys. D: Appl. Phys.* **49** 105301

View the [article online](#) for updates and enhancements.

You may also like

- [Preparation of \$\text{Ca}_{0.5}\text{Zr}_2\(\text{PO}_4\)_3\$ and \$\text{Ca}_{0.45}\text{Eu}_{0.05}\text{Zr}_2\(\text{PO}_4\)_3\$ nanopowders: structural characterization and luminescence emission study](#)
L Alcaraz, J Isasi, C Díaz-Guerra *et al.*
- [Magnetically driven magnetostructural transformations of shape memory alloys](#)
V A L'vov, E Cesari, J I Pérez-Landazábal *et al.*
- [Modeling stochasticity in biochemical reaction networks](#)
P H Constantino, M Vlysidis, P Smadbeck *et al.*



ECS
The
Electrochemical
Society
Advancing solid state &
electrochemical science & technology

DISCOVER
how sustainability
intersects with
electrochemistry & solid
state science research

The nature of graphene–metal bonding probed by Raman spectroscopy: the special case of cobalt

Inés Serrano-Esparza^{1,2}, Jiyu Fan^{1,2,4}, Jan M Michalik^{1,2,5},
Luis Alfredo Rodríguez^{3,6}, Manuel Ricardo Ibarra^{2,3}
and José María de Teresa^{1,2,3,7}

¹ Instituto de Ciencia de Materiales de Aragón, Facultad de Ciencias, Universidad de Zaragoza–CSIC, 50009 Zaragoza, Spain

² Departamento de Física de la Materia Condensada, Universidad de Zaragoza, 50009 Zaragoza, Spain

³ Laboratorio de Microscopías Avanzadas (LMA), Instituto de Nanociencia de Aragón (INA), Universidad de Zaragoza, 50018 Zaragoza, Spain

E-mail: deteresa@unizar.es

Received 15 September 2015, revised 16 December 2015

Accepted for publication 18 December 2015

Published 3 February 2016



CrossMark

Abstract

The nature of graphene–metal bonding is crucial for the performance of graphene-based electronic devices. Raman spectroscopy is a powerful technique for probing the electronic behaviour of graphene–metal interfaces. The changes in the Raman spectrum of pristine graphene upon contact with standard metal layers are reported here. In particular, the study is focused on metallization by electron-beam evaporation using chromium or titanium (commonly used as an adhesion layer to improve the bonding of other metals such as gold) and nickel or cobalt (ferromagnetic materials used for spintronics). The results obtained indicate that the main changes in the Raman spectra can be explained in terms of a biaxial strain generated by graphene trying to match the crystalline lattice of the metal. In the case of cobalt, we find that the strong binding of some cobalt atoms to graphene generates a spectrum with a duplication of the characteristic graphene peaks: those corresponding to cobalt physisorbed to graphene and those corresponding to cobalt chemisorbed to graphene, strongly redshifted. Such special behaviour of the graphene–cobalt interface is correlated to the low contact resistance and the enhanced perpendicular magnetic anisotropy of cobalt on graphene.

Keywords: graphene–metal interface, Raman spectroscopy, cobalt chemisorptions, electrical devices

 Online supplementary data available from stacks.iop.org/JPhysD/49/105301/mmedia

(Some figures may appear in colour only in the online journal)

⁴ Present address: Department of Applied Physics Nanjing University of Aeronautics and Astronautics, Nanjing 210016, People's Republic of China.

⁵ Present address: Department of Solid State Physics, Faculty of Physics and Applied Computer Science, AGH University of Science and Technology, al. A. Mickiewicza 30, 30-059 Kraków, Poland.

⁶ Present address: CEMES—CNRS 29, rue Jeanne Marvig, B.P. 94347 F-31055, Toulouse Cedex, France.

⁷ Author to whom any correspondence should be addressed.

1. Introduction

Graphene, a single layer of carbon atoms arranged in a hexagonal lattice, was recently discovered despite the assumption that 2D crystals could not exist [1]. Its properties seem to be unequalled: thin but strong material, flexible, excellent conductivity, impermeable to gases, its electrons follow the

Dirac equation, which means they behave in a relativistic way, etc [2]. All these properties make graphene a promising material for industry and open up a broad field of study for many applications in fields such as aeronautics, the automobile industry, electronics, energy storage, communications, sensors, solar panels, etc [3]. Most applications for electronics require a lithography process and subsequent metallization. These metals, generally deposited by sputtering or electron beam evaporation, can induce changes in graphene: doping [4–6], strain [7] or introducing defects and disorder [8, 9]. Such changes can be detrimental with respect to the properties exhibited by pristine graphene [10, 11]. Raman spectroscopy is a powerful technique for investigating such changes in graphene [12].

Raman scattering reflects an inelastic dispersion of light by matter, caused by phonons or vibrational modes. In the case of graphene, despite its nanometric dimensions, electronic resonances make the Raman signal intense enough to be detected. Typical peaks found in graphene spectra are the following [8, 12]:

- The G peak is attributed to the stretching of sp^2 bonds, with a net momentum transfer close to zero ($\Delta q \approx 0$).
- The D peak comes from longitudinal optical phonons around K ($\Delta q \approx K$), i.e. it stems from an inter-valley transition, activated by defects.
- The 2D peak is the second order of the D peak, generated by two phonons with opposite momentum which results in a total momentum close to zero, and hence permitted by Raman selection rules.

These peaks are very sensitive to change such as doping, stress or number of layers in the graphene [8, 12]. Doping is defined as the addition of impurities to a semiconductor in such a way that the semiconductor gets an excess of charge, positive (P-doping) or negative (N-doping) [13]. Analogously, doped graphene refers to an excess of holes or electrons, where the Fermi level lies in the valence band or in the conduction band respectively. Doping can have its origin in the addition of impurities or in charge transfer due to contact with a metal. When two metals have different work functions (WFs)—energy difference from the Fermi level to the vacuum level—there is an electron transfer from the metal with lower WF to the one with higher WF, with a consequent N-doping of the latter. Graphene, with a WF of 4.5 eV, will become P-doped when in contact with cobalt (5.0 eV) or nickel (5.04 eV), whereas it will become N-doped when in contact with titanium (4.33 eV) [14] and barely doped when in contact with Cr (4.5 eV). Other studies show, however, a 0.7 eV transfer from a cobalt adatom to monolayer graphene [15], opposite to what is expected in terms of WF. In a Raman spectrum, doping is manifested by a shift in the G and 2D peaks: the G peak blue-shifts for both electron and hole doping, whereas the 2D peak red-shifts for electron doping and blue-shifts for hole doping. Moreover, the FWHM (full width at half maximum) of G peaks decreases significantly with doping (from 15 cm^{-1} to 8 cm^{-1}) and the ratio between the intensities of the G and 2D peaks decreases from 3.5 to values close to 1 [4–6].

Another relevant issue in graphene–metal contact is strain. Strain occurs in a crystal when its symmetry axes are

deformed out of equilibrium. In graphene, a 2D crystal, the strain tensor is quite simple and can be studied theoretically [7, 12]. The Raman spectrum is very sensitive to strain, as any deformation will modify the vibrational modes. In the case of the G peak, a uniaxial strain will generate a difference between the vibrations along the strain axis and those transverse to it. As a consequence, the uniaxial strain will split the G peak into two components with an FWHM that remains unchanged at 12 cm^{-1} . In the case of biaxial strain, the G peak does not split because there is no difference between directions. Additionally, both the G and 2D peaks will undergo a red-shift.

Finally, other effects such as vacancies in the crystalline structure, impurity implantation and wrinkles can cause disorder in the crystalline structure, and symmetry breaking. Graphene is very sensitive to symmetry breaking and this is reflected in the phonon dispersion relation and, hence, in the Raman spectrum [12]. In particular, as we mentioned before, two new peaks, previously forbidden due to Raman selection rules ($q = 0$), appear at 1360 cm^{-1} (D) and 1620 cm^{-1} (D'). Moreover, the ratio between the intensities of the G and D peaks increases with the number of defects, all peaks broaden with an FWHM higher than 15 cm^{-1} and the G peak suffers a blue-shift [9]. If the G peak broadens enough, it could even merge into a single peak centred at 1600 cm^{-1} [8, 9].

One should consider all these changes when studying graphene. Ideally, pristine samples should be free from any defect, strain or doping. However, interaction with the substrate can modify their properties. From the procedures available for isolating graphene [16], mechanical exfoliation is still the one that produces graphene with better electronic quality. We will then focus on this type of sample, exfoliated on SiO_2 , only slightly doped and nearly free from defects. An initial study is necessary for a better understanding of the interaction between graphene and different metals. We will use Cr and Ti, because they are used for metallization [17], and Co and Ni for their general use in spintronics [18]. In particular, it was recently shown that graphene enhances the perpendicular magnetic anisotropy in a stack of graphene, Co and Ir(111) [19, 20].

At this point, previous literature directly related to the present experiments should be introduced. It is worth mentioning that the behaviour of Cr and Ti on CVD graphene has been investigated [21], but the behaviour observable with exfoliated graphene, as investigated here, can be significantly different due to the superior electronic properties of exfoliated graphene. Other work has focused on the behaviour of graphene when deposited on Co, Ni or Pd substrates [22–24], which contrasts with frequent experimental situations in which metallization takes place after graphene growth. Theoretical studies of the doping caused by metals on graphene also exist [25]. Interestingly, [26] studies the interaction of Co, Ni and other metals on mechanically exfoliated graphene, finding that doping is the main effect after cobalt and nickel metallization of graphene. However, the absence of an initial study of doping in pristine samples, which is crucial for the correct interpretation of the results, calls for a specific study as carried out here. In the present work, we perform complete

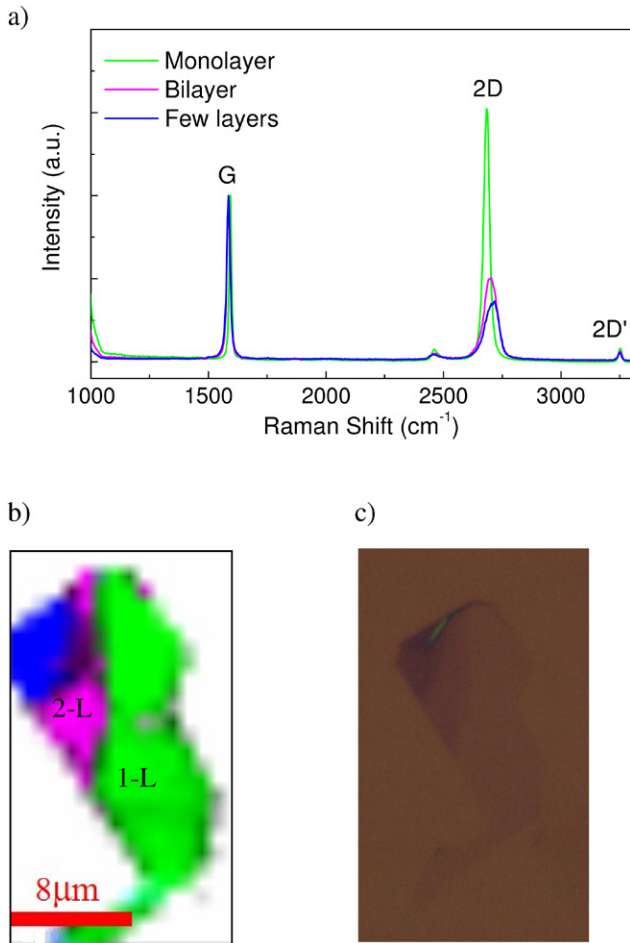


Figure 1. (a) Raman spectra normalized to the intensity of the G peak of a graphene flake with different number of layers. Each spectrum is the average over all spectra taken in a certain area, with the same colour in image (b), where one spectrum is taken with a one-micron step. The white background corresponds to the SiO_2 background and the labels on each area indicate the number of layers. (c) Optical image of the same graphene flake.

characterization of pristine graphene and the possible effects of metal deposition (doping, defect, or strain) using Raman spectroscopy. In the case of cobalt, transmission electron microscopy (TEM) investigations were needed to complete the characterization, thus obtaining better understanding of the results.

2. Experiment

2.1. Sample preparation

Graphene was mechanically exfoliated from highly oriented pyrolytic graphite (HOPG) using the standard Scotch[®] tape method [1]. We used a commercial Si/SiO₂ substrate with nominally 300 nm of SiO₂, thermally oxidized from a Si wafer. The substrate was previously activated by oxygen plasma for 15 min in order to improve the adhesion of graphene to the substrate. Once the graphene was deposited, we searched for monolayer or few-layer graphene using an optical microscope. Despite being one atom thick, graphene is visible under white light because it introduces strong amplitude modulation

in the interface air–graphene–SiO₂ [27]. The optical contrast changes abruptly from monolayer to bilayer, trilayer or HOPG, hence, from optical inspection of the sample, the number of layers in the flakes can be estimated. Nevertheless, in order to come to accurate conclusions, one should obtain the Raman spectrum and analyse the position, intensity and width of the different peaks. Finally, for metal evaporation, we used an electron beam evaporator BOC Edwards Auto 500, which works under a vacuum of 10^{-6} mbar and 5 kV power supply.

2.2. Raman measurements and analysis

Raman spectroscopy is a fast and non-invasive technique that allows the deep and broad study of graphene properties. We used a Confocal Raman Alpha 300 M+ from WITec, which combines a Raman spectrograph with a confocal microscope. There are different lasers available in the system, and unless specified, we used a 532 nm laser wavelength λ_{LASER} , with a spot size of 1 μm and an adjustable power fixed at 1 mW to avoid sample heating.

A confocal microscope limits the incoming radiation becoming out of focus and so the signal has better quality, allowing a smaller lateral resolution than conventional optical microscopes, necessary for nanostructures. The version employed also has an automatic motorized sample positioner in the x -, y - and z -directions that allows 2D and 3D mapping. For our purposes, we performed 2D mapping. The integration time was fixed from 0.7 s for pristine samples to 4 s for some metallized samples, where the signal is much smaller. WITec software can process these spectra selecting those with similar characteristics and taking the average, with which we can diminish the isolated irregularities and obtain averaged results.

2.3. Electron microscopy

In the case of cobalt metallization, the crystalline structure of cobalt over graphene was studied using the high resolution transmission electron microscopy (HRTEM) technique. For this study, TEM lamellae were prepared to perform a cross-sectional analysis of all layers. These lamellae were fabricated using the standard TEM lamella preparation method [28] in a focused ion beam—scanning electron microscopy (SEM) equipment (Helios 600) from FEI. HRTEM experiments were carried out in a Titan Cube 60–300, from FEI, and operated at 300 kV. This electron microscope is equipped with a SuperTwin[®] objective lens and a CETCOR Cs-objective corrector from CEOS Company, allowing a spatial resolution of 0.08 nm.

3. Results

Raman spectra of graphene flakes mechanically exfoliated over SiO₂ were first studied, mapping the whole flake and taking a spectrum with a one-micron step. As an example, figure 1 shows a typical spectrum taken with the Raman equipment in

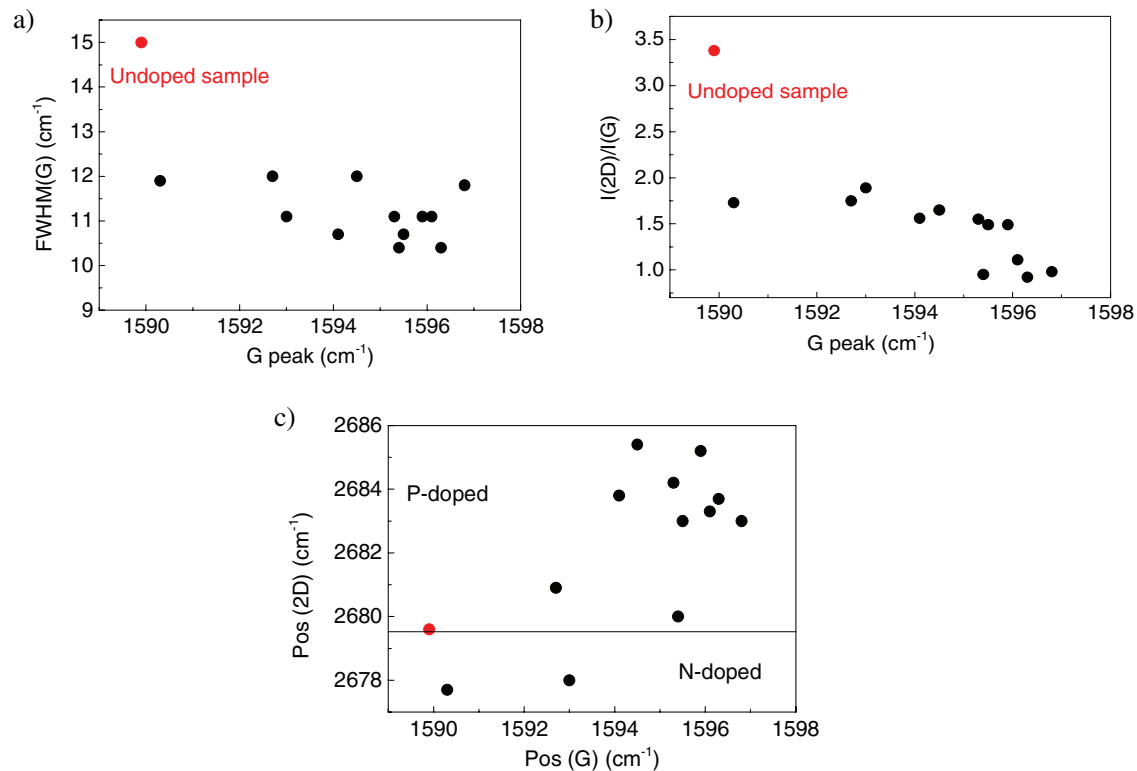


Figure 2. Doping effects in pristine graphene can be tracked through the features exhibited by the characteristic Raman peaks: (a) FWHM of the G peak as a function of the G peak position. (b) Ratio between intensities of the 2D and G peaks as a function of position of the G peak. The ratio close to 3.5 (coloured dot) means that it is an undoped sample. Moreover, the decrease in the FWHM of the G peak, the blue-shift of its position and the lower ratio between intensities imply that the other samples are doped. (c) Position of the 2D peak as a function of the G peak position. Whereas a blue-shift in the G peak is a feature from both N- and P-doping, a red-shift in the 2D peak means N-doping and vice versa. Therefore, most of our pristine graphene samples are initially P-doped.

a graphene flake with different numbers of layers. The software of the equipment clustered the spectra into three groups comparing the 2D peak and performing the average spectra shown in figure 1. After fitting the 2D peak to a certain number of Lorentz curves, it can be concluded that they correspond to monolayer (green), bilayer (magenta), and few-layer graphene (dark blue).

In addition, the software allows the display, with the same colour, of the areas with similar spectra. Thus, the green area in figure 1 corresponds to monolayer, magenta to bilayer and dark blue to few-layer graphene (the white area is the SiO₂ substrate). The average over a certain area gives us the certitude that the behaviour measured is present in the entire surface and not only at one point. Therefore, the absence of disorder peaks (D and D') in the averaged spectra confirms the good quality of exfoliated graphene with respect to defects.

As graphene is deposited on a substrate, generally SiO₂, it is not completely isolated and, although free from defects, it is usually slightly doped. Doped graphene has an FWHM for the G peak much lower than 15 cm⁻¹ and a ratio between the 2D and G peak intensities much lower than 3.5 [4, 9]. Only one sample in figure 2 (represented by a red dot) is undoped, as it has an FWHM(G) around 15 cm⁻¹—this means between 1.25 and 1.4 times higher than other samples—and a ratio $I(2D)/I(G)$ of 3.38—almost twice the ratio for other samples. The fact that the G peaks for the presumed doped samples are blue-shifted with respect to the undoped one confirms our hypothesis. So, we can use this sample as a reference to

determine whether the other samples are P-doped or N-doped by inspection of the position of the 2D peak. Samples with a 2D peak blue-shifted with respect to the reference sample are P-doped whereas they are N-doped for a red-shifted 2D peak (see figure 2(c)). In general, the data suggest that our pristine graphene samples are P-doped after deposition onto SiO₂.

As previously mentioned, it is of great importance to know the initial doping of the pristine graphene samples to explain the subsequent changes in the Raman spectra of the same samples after metallization. Table 1 summarizes the results obtained for several metals (for more details, see the supporting information (stacks.iop.org/JPhysD/49/105301/mmedia)). The first column shows the change in the position of the G peak, i.e. the final position minus the original position. All G peaks undergo a red-shift. The higher red-shift is obtained for titanium, whereas chromium seems to affect the graphene less. Similarly, 2D peaks are red-shifted for all metals. Chromium and titanium metals have less effect than cobalt and nickel, which have a similar change in the position of their peaks. The third and fourth columns show the final FWHM(G) and $I(2D)/I(G)$. FWHM(G)s is higher than 15 cm⁻¹ in all cases and $I(2D)/I(G)$ decreases considerably compared to the pristine spectra. On the one hand, titanium is, for FWHM(G) and $I(2D)/I(G)$, the more influencing metal with an FWHM(G) around 109 cm⁻¹ and $I(2D)/I(G)$ much lower than 1, despite the red-shift being similar to other metals. On the other hand, FWHM(G) for

Table 1. Changes in the position of the G and 2D peaks, the FWHM of the G peak, and the ratio between the 2D and G peak intensities after the evaporation of 3 nm of different metals by electron beam evaporation.

Metal	$\Delta\text{Pos (G) (cm}^{-1}\text{)}$	$\Delta\text{Pos (2D) (cm}^{-1}\text{)}$	FWHM (G) (cm ⁻¹)	$I(2D)/I(G)$
Cobalt	-11 ± 5	-30 ± 5	36 ± 11	0.74 ± 0.04
Nickel	-16.6 ± 0.6	-25.0 ± 1.6	31.2 ± 1.6	0.69 ± 0.07
Chromium	-10.75 ± 0.15	-11.9 ± 0.02	23.0 ± 0.1	1.34 ± 0.03
Titanium	-34 ± 4	-7 ± 3	109 ± 3	0.45 ± 0.19

Note: The shifts in the G and 2D peaks, along with a decrease in $I(2D)/I(G)$ can be interpreted as due to the presence of doping in graphene. However, the shift expected for some metals is the opposite of what is measured: that the red-shift found in all peaks is indeed explained in terms of a biaxial strain in graphene. Moreover, the appearance of D and D' peaks, as shown in figure 3, and the broadening of the peaks imply the presence of disorder, induced during the metal evaporation.

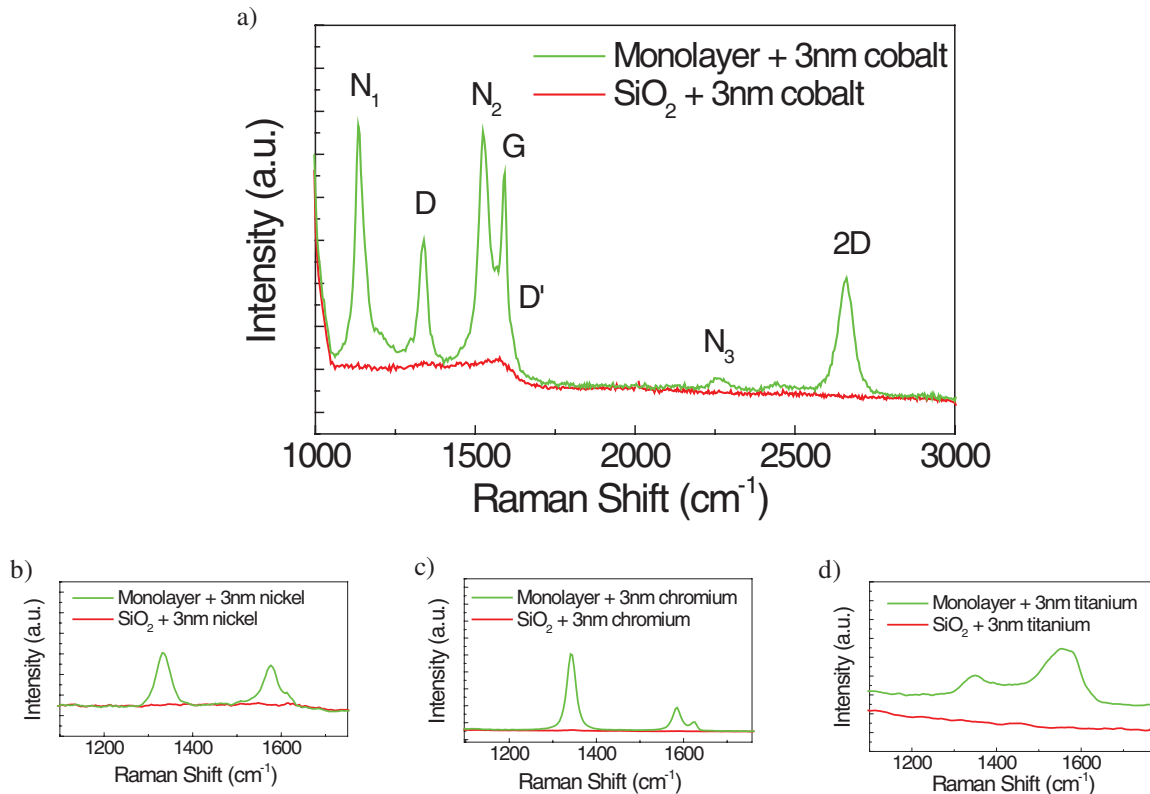


Figure 3. (a) Raman spectrum of a graphene flake after deposition of 3 nm of cobalt. Contrary to other metals (b)–(d), two new peaks are noticed in the spectrum, called N_1 and N_2 at 1137 cm^{-1} and 1527 cm^{-1} respectively, and a third one N_3 at 2267 cm^{-1} that is present in some spectra, which do not correspond to the cobalt spectrum itself. In all cases, we performed the average of all the spectra taken over the flakes. Raman spectra after evaporation of 3 nm of (b) Ni, (c) Cr, and (d) Ti are shown.

the chromium samples is slightly higher than 15 cm^{-1} and $I(2D)/I(G)$ remains above one. This set of results indicates that they cannot be simply explained by doping effects caused by the difference between the graphene work function and that of the respective metal. Instead, it implies that the main contribution of growing metals on graphene is the occurrence of strain, which appears as a red-shift in both the G and 2D peaks; see the discussion section for more detail. The appearance of disorder peaks, D and D', as shown in figure 3, and the broadening of some peaks reveal the introduction of defects during the metallization.

Disorder peaks appear in all spectra, as shown in figure 3. However, in the case of cobalt evaporation (figure 3(a)), two additional peaks, N_1 and N_2 , at 1137 cm^{-1} and 1527 cm^{-1} , respectively, were found in the sample shown. A third peak

N_3 , at 2267 cm^{-1} in figure 3(a), is found in some of the spectra, although N_1 and N_2 are more intense. The spectrum of cobalt over SiO_2 confirms that they do not belong to the cobalt spectrum itself, as seen in figure 3(a), and that they are also missing in other metals' spectra. Their origin must be entirely due to an interaction between graphene and cobalt atoms. To better understand the origin of these new peaks and their persistence, we carried out some further studies, changing the number of layers and measuring over long periods of time. In figure 4, it is shown that the new peaks are present up to few-layer graphene with approximately the same intensity and positions (see table S2 in the supporting information (stacks.iop.org/JPhysD/49/105301/mmedia)).

Evolution over 12 weeks, shown in figure 5, indicates that the new peaks remain with the same or even higher intensity,

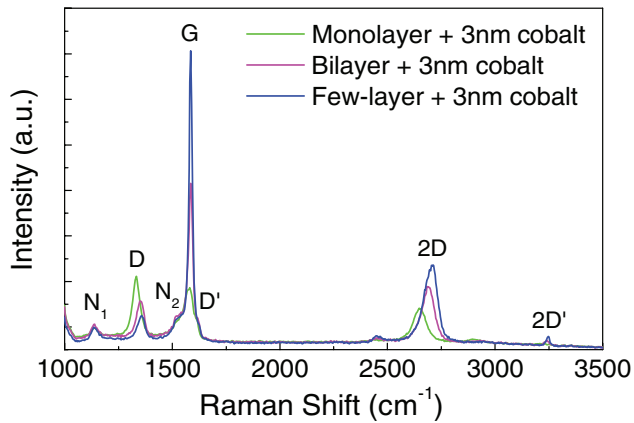


Figure 4. The new peaks, N_1 and N_2 , of the cobalt–graphene system are independent of the number of graphene layers. We can conclude that the new peaks are due to an interfacial interaction between cobalt and the first layer of carbon atoms.

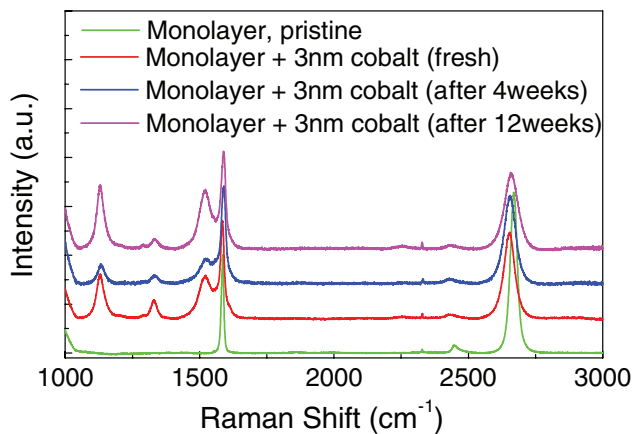


Figure 5. Evolution of spectra over time after the deposition of 3 nm of cobalt, normalized to the G peak. Due to the absence of differences between them, we can conclude that the interaction between cobalt and graphene is independent of time, corresponding to a stable cobalt–graphene bonding.

and the positions remain unchanged (see table S3 in the supporting information (stacks.iop.org/JPhysD/49/105301/mmedia)). This implies that the effect producing the new peaks survives with time, contrary to other peaks: the D peak tends to disappear after twelve weeks (defect healing), whilst the G peak and 2D peaks move towards higher frequency positions, suggesting that strain decreases. The results thus point to bonding effects between graphene and cobalt as the origin of the phenomenon. Let us also point out that the intensity of the new peaks with respect to the G and 2D peaks varies with the sample, as we can see in the spectra of figures 3–5.

As a consequence, we studied the crystal structure of cobalt using TEM. The cobalt layer, marked between two lines, is continuous along the sample with an actual width of 5 nm (figure 6). The amorphous structure corresponds to SiO_2 , whereas the crystalline structure forming nanoparticles over cobalt is the platinum deposited using the focused-electron beam-induced deposition method to protect cobalt from ion irradiation during lamella preparation. In the HRTEM image, graphene is impossible to differentiate from cobalt and SiO_2 because of its one atom thickness and the intrinsic

roughness of the sample. We found that cobalt forms a polycrystalline structure with small grains of size around 5 nm. Complementary information of the crystal structure of the cobalt grains was obtained by performing fast Fourier transforms (FFTs) on certain areas of the HRTEM image, where the small grains showed planes and atomic positions. The FFTs display white points that correspond to the diffraction planes of the lattice. We have delimited concentric yellow circumferences that pass through the most intense diffraction points to estimate the d-spacing in each plane. If we compare the d-spacing measured using a FFT with those accepted in the literature [29], we can conclude that cobalt crystallizes in an hcp structure, where the d-spacings are: 1.15 Å for (1 0 3) plane, 1.25 Å for (1 1 0), 1.48 Å for (1 0 2), 2.03 Å for (0 0 2) and 2.17 Å for (1 0 0).

4. Discussion

We found that our pristine samples are initially doped, in general by holes, due to interaction with the substrate. The undoped sample shows an FWHM of the G peak close to 15 cm^{-1} , a ratio between intensities of the 2D and G peaks of around 3.5 and the position of the G peak is at 1590 cm^{-1} . The other samples are blue-shifted for the G peak and have lower FWHM of the G peak and lower $I(2D)/I(G)$ ratios, a signature of doped graphene. Finally, the position of 2D peak with respect to that of the undoped sample allows us to determine whether the other samples are P-doped or N-doped.

As most samples are doped before treatment, the charge transfer produced after metallization can generate extra doping that can be investigated through the position of the 2D peak. The 2D peak always blue-shifts for P-doping and red-shifts for N-doping, independently of the initial doping. Moreover, the G peak blue-shifts provided that the sample was previously un-doped but if the sample was doped, the expected shift would depend on whether the sample was initially P- or N-doped and whether the doping crosses the Dirac point. We should also consider the strain effect and the disorder; the interpretation of the shift in the G peak is consequently complex. In table 1, one can see that both the 2D and G peaks red-shift for all metals, independently of the expected doping due to the difference in the work function. Both doping and defects produce a blue-shift in the G peak [9], contrary to strain, which generates a red-shift [7]. Therefore, a red-shift in the G peak shows that the contribution of a biaxial strain generated during the evaporation exceeds that of strain and doping, although it is difficult to determine which metal produces a higher strain. In general, chromium is the metal that affects graphene the least, being a better choice than titanium for making a metal contact. Nickel and cobalt both generate similar effects on graphene: a red-shift in the G peak around 16 cm^{-1} and in the 2D peak around 25 cm^{-1} , the FWHM of the G peak increases up to 30 cm^{-1} , and the $I(2D)/I(G)$ ratio decreases down to approximately 0.7. Finally, the presence of D and D' along with the broadening of the other peaks indicate that the metallization induces disorder in the crystalline structure of graphene.

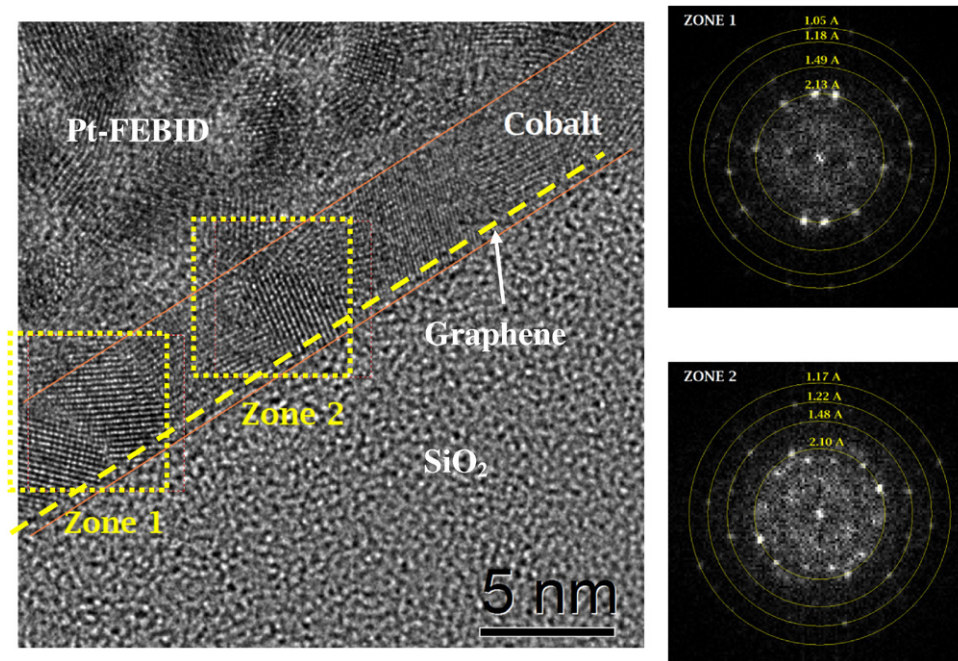


Figure 6. Left: HRTEM images of a cross-section lamella of the cobalt–graphene system. Right: FFT images extracted from the marked zones of the HRTEM images. We conclude that cobalt is polycrystalline with 5 nm grain size and showing an hcp crystal structure.

The most interesting result is the appearance of new peaks, as revealed in figure 3(a), that are independent of the cobalt evaporation on graphene. As seen in figure 5, these peaks do not change with time. The dependence of the peaks on the number of layers is negligible (see table S2) (stacks.iop.org/JPhysD/49/105301/mmedia). Whereas the D and 2D peaks blue-shift with the number of layers, the new peaks stay at the same position and with similar intensity. What is the origin of such peaks? In [26], the authors found a shoulder in the G peak in both Ni and Co spectra at $\sim 1545\text{ cm}^{-1}$, which they called the G' peak, and that they attribute to ‘phonon-induced intraband electronic transitions’ [30]. However, in our case, this peak is much more intense than in that paper, placed at lower frequencies ($\sim 1525\text{ cm}^{-1}$) and is accompanied by two additional peaks (N_1 and N_3). We propose an alternative interpretation as discussed below.

We recall that when graphene is grown on a certain metal, it can be physisorbed, with a large binding distance, or chemisorbed, with a small binding distance. This is a consequence of the hybridization between the π bonds of graphene and the d bonds in the surface of the metal, related to the occurrence or not of direct matching between lattices [22]. As an example, graphene physisorbs on Pt(1 1 1) and Ir(1 1 1) but chemisorbs on Ni(1 1 1) and Co(0 0 1) [22]. In our case, the metal is on top of graphene, but the physics is the same: some atoms of cobalt could be chemisorbed on graphene generating new vibrational modes. Our TEM study indicates that the crystalline structure of cobalt is in the hexagonal phase, with grains of around 5 nm (figure 6). In [22] the authors study the phonon dispersion of graphene with chemisorbed nickel and find a softening of the optical branches as a consequence of the stretching of graphene, producing around 100 cm^{-1} of red-shift in the Raman spectra [22]. Another important effect shown in that paper is

the suppression of the Kohn anomalies because of the hybridization between the π bonds of graphene and the d bonds in the metal. This suppression implies a decrease in the dispersion of the D and 2D peaks with laser energy in the case of weak interaction. For high interaction, the Raman signal disappears because the bonds between graphene and nickel lead to a loss of resonance. Let us suppose that we can apply such Raman results in Ni(111) to Co(0001). If we had chemisorbed cobalt atoms on monolayer graphene, we could also consider the N-doping suggested in [15], which would also produce a red-shift in the 2D peak, as observed.

If, as suggested by the TEM results, only some cobalt grains are properly orientated for the π –d hybridization, only atoms belonging to such grains will be chemisorbed on graphene. Graphene in those areas would have different Raman spectra from other areas with physisorbed cobalt and, as a consequence, the total Raman spectrum will be a superposition of both. Such cobalt chemisorption would be enough to have a softening of the optical branches but not so intense for the total disappearance of the Raman peaks. As a consequence of the softening, the G peak would move towards lower energies and so would the D peak, which would be replaced by N_2 and N_1 respectively; the 2D peak would in fact be N_3 . The differences in the intensity of these peaks with respect to the G and 2D peaks as a function of the sample would be related to the ratio between chemisorbed and physisorbed cobalt on graphene. The higher the number of chemisorbed cobalt atoms, the more intense the new peaks with respect to the G peak. Therefore, N_3 , the weaker peak, is only present in some spectra with an elevated contribution of these new peaks (for example in figure 3(a) but not in figure 4).

For the D peak, we see no dependence of N_1 on the number of layers (figure 4), whereas for pristine graphene we see a

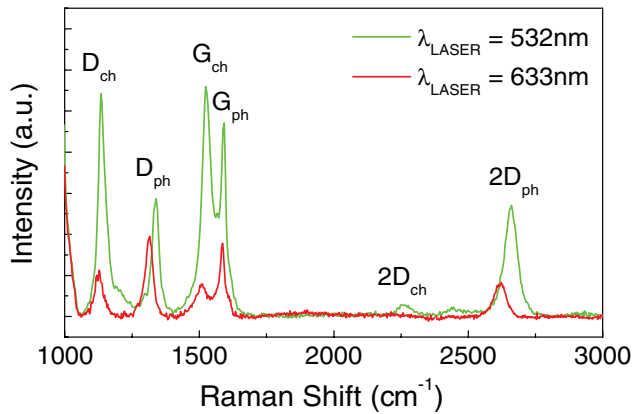


Figure 7. Green line: the same spectrum shown in figure 3(a) with wavelength of 532 nm is displayed together with the interpretation of each peak. We suggest the superposition of two contributing spectra, corresponding respectively to physisorbed and chemisorbed cobalt on graphene. Each peak is labelled with a sub-index ph for the physisorbed cobalt and ch for chemisorbed cobalt. Red line: the spectrum using 633 nm wavelength is shown. The dispersion of the new peaks with the laser wavelength is smaller than the dispersion in peaks D_{ph} and $2D_{ph}$, which is a consequence of a reduction in the Kohn anomaly.

blue-shift with the number of layers (peak D in figure 4). This means the origin of the new peaks is an interfacial interaction between the graphene and the cobalt. Finally, in [22] it is stated that the reduction of the Kohn anomaly—due to the charge transfer between graphene and the metal due to the chemisorption of graphene—can be detected by the reduction of the dispersion of the D and $2D$ peaks with laser frequency. From now on, let us label with a sub-index ‘ph’ or ‘ch’ those peaks corresponding to physisorbed or chemisorbed cobalt on graphene, respectively. We performed new Raman measurements using another laser source with a wavelength of 633 nm. In figure 7, the change in the frequency of the D_{ch} peak when measured at 633 nm with respect to that at 532 nm is much smaller than that of the D_{ph} and $2D_{ph}$ peaks. Unfortunately, the $2D_{ch}$ peak is not observed using the 633 nm laser. The reduction of the dispersion in the D peak is the best proof of the hybridization between the π bonds in graphene and the d bonds in cobalt.

We also deposited nickel on graphene but did not observe the new peaks. After HRTEM measurements (see supporting information (stacks.iop.org/JPhysD/49/105301/mmedia)), we concluded that the nickel was probably grown forming grains in its hexagonal (hcp) phase, mainly oriented in faces (002) and (101) towards the graphene–nickel interface. This means there are no nickel grains on the graphene surface with crystal orientation (111) and the chemisorption is not viable. To have the superposition of the two spectra the chemisorption must be weak, but strong enough to see the new peaks. Thus, these subtle conditions seem to be present only in the case of cobalt.

5. Conclusions

To conclude, we have shown that after metallization of graphene with different metals, the main contribution to changes in the spectra is biaxial strain due to the graphene trying to accommodate the metal crystalline structure. In the case of

cobalt, there is a better matching of its unit cell and that of graphene with the accompanying hybridization of the metal d orbitals with the π orbitals in graphene. Note that this hybridization is the origin of an enhanced perpendicular magnetic anisotropy in graphene–Co–Ir (111) stacks [19, 20] and the good quality (Ohmic contacts with a low contact resistance) contacts made in cobalt [31] and nickel [32]. In our experimental conditions, only some Co grains chemisorb on graphene, leading to a spectrum red-shifted compared to that of physisorbed grains, and thus a duplication of the peaks, generated both by the match of the lattice [22] and the N-doping [15]. Our results highlight the subtlety of the electronic interaction between graphene and evaporated metals, which is crucial for the understanding of their adhesion and the properties shown by graphene, with important technological implications.

Acknowledgments

This work was supported by the Spanish Ministry of Economy and Competitiveness through project No. MAT2011-27553-C02 including FEDER funds, and by the Aragon Regional Government. Experimental help from Íñigo Echániz of ‘Instituto de Nanociencia de Aragón’ (INA) and the clean-room technicians of ‘Laboratorio de Microscopías Avanzadas’ (LMA) is warmly acknowledged.

Appendix. Supporting information

Extra information on HRTEM images and FFT measurements of the nickel–graphene interface is accessible in the supporting information, along with raw data and fitting parameters for the metalized samples (stacks.iop.org/JPhysD/49/105301/mmedia).

References

- [1] Novoselov K S, Geim A K, Morozov S V, Jiang D, Zhang Y, Dubonos S V, Grigorieva I V and Firsov A A 2004 Electric field effect in atomically thin carbon films *Science* **306** 666–9
- [2] Geim A K 2009 Graphene: status and prospects *Science* **324** 1530–4
- [3] Ferrari A C *et al* 2015 Science and technology roadmap for graphene, related two-dimensional crystals, and hybrid systems *Nanoscale* **7** 4598–810
- [4] Das A *et al* 2008 Monitoring dopants by Raman scattering in an electrochemically top-gated graphene transistor *Nat. Nanotechnol.* **3** 210–5
- [5] Yan J, Zhang Y, Kim P and Pinczuk A 2007 Electric field effect tuning of electron–phonon coupling in graphene *Phys. Rev. Lett.* **98** 166802
- [6] Pisana S, Lazzeri M, Casiraghi C, Novoselov K S, Geim A K, Ferrari A C and Mauri F 2007 Breakdown of the adiabatic Born–Oppenheimer approximation in graphene *Nat. Mater.* **6** 198–201
- [7] Mohiuddin T M G *et al* 2009 Uniaxial strain in graphene by Raman spectroscopy: G peak splitting, Grüneisen parameters, and sample orientation *Phys. Rev. B* **79** 205433
- [8] Ferrari A C 2007 Raman spectroscopy of graphene and graphite: disorder, electron–phonon coupling, doping and nonadiabatic effects *Solid State Commun.* **143** 47–57

- [9] Casiraghi C, Pisana S, Novoselov K S, Geim A K and Ferrari A C 2007 Raman fingerprint of charged impurities in graphene *Appl. Phys. Lett.* **91** 233108
- [10] Banhart F, Kotakoski J and Krasheninnikov A V 2011 Structural defects in graphene *ACS Nano* **5** 26–41
- [11] Peres N M R, Guinea F and Castro Neto A H 2006 Electronic properties of disordered two-dimensional carbon *Phys. Rev. B* **73** 125411
- [12] Jorio A, Dresselhaus M S, Dresselhaus G F and Saito R 2011 *Raman Spectroscopy in Graphene Related Systems* (Weinheim: Wiley)
- [13] Kittel C 2005 *Introduction to Solid State Physics* ed S Johnson *et al* (New York: Wiley)
- [14] Anonymous 2008 *CRC Handbook of Chemistry and Physics* (Boca Raton, FL: CRC Press) pp 12–114
- [15] Zhang G P, Liu X, Wang C Z, Yao Y X, Zhang J and Ho K M 2013 Electronic and spin transport properties of graphene nanoribbon mediated by metal adatoms: a study by the QUAMBO-NEGF approach *J. Phys.: Condens. Matter* **25** 105302
- [16] Bonaccorso F, Lombardo A, Hasan T, Sun Z, Colombo L and Ferrari A C 2012 Production and processing of graphene and 2D crystals *Mater. Today* **15** 564–89
- [17] Evans A G, Hutchinson J W and Wei Y 1999 Interface adhesion: effects of plasticity and segregation *Acta Mater.* **47** 4093–113
- [18] Karpan V M, Khomyakov P A, Starikov A A, Giovannetti G, Zwierzycki M, Talanana M, Brocks G, Van Den Brink J and Kelly P J 2008 Theoretical prediction of perfect spin filtering at interfaces between close-packed surfaces of Ni or Co and graphite or graphene *Phys. Rev. B* **78** 1–11
- [19] Rougemaille N, N'Diaye A T, Coraux J, Vo-Van C, Fruchart O and Schmid A K 2012 Perpendicular magnetic anisotropy of cobalt films intercalated under graphene *Appl. Phys. Lett.* **101** 1–3
- [20] Vo-Van C *et al* 2010 Ultrathin epitaxial cobalt films on graphene for spintronic investigations and applications *New J. Phys.* **12** 1–14
- [21] Iqbal M W, Singh A K, Iqbal M Z and Eom J 2012 Raman fingerprint of doping due to metal adsorbates on graphene *J. Phys.: Condens. Matter* **24** 335301
- [22] Allard A and Wirtz L 2010 Graphene on metallic substrates: suppression of the Kohn anomalies in the phonon dispersion *Nano Lett.* **10** 4335–40
- [23] Batzill M 2012 The surface science of graphene: metal interfaces, CVD synthesis, nanoribbons, chemical modifications, and defects *Surf. Sci. Rep.* **67** 83–115
- [24] Eom D, Prezzi D, Rim K T, Zhou H, Lefenfeld M, Xiao S, Nuckolls C, Hybertsen M S, Heinz T F and Flynn G W 2009 Structure and electronic properties of graphene nanoislands on Co(0001) *Nano Lett.* **9** 2844–8
- [25] Giovannetti G, Khomyakov P, Brocks G, Karpan V, van den Brink J and Kelly P 2008 Doping graphene with metal contacts *Phys. Rev. Lett.* **101** 026803
- [26] Wang W X, Liang S H, Yu T, Li D H, Li Y B and Han X F 2011 The study of interaction between graphene and metals by Raman spectroscopy *J. Appl. Phys.* **109** 07C501
- [27] Roddaro S, Pingue P, Piazza V, Pellegrini V and Beltram F 2007 The optical visibility of graphene: interference colors of ultrathin graphite on SiO₂ *Nano Lett.* **7** 2707–10
- [28] Giannuzzi L A and Stevie F A 2005 *Introduction to Focused Ion Beams* (Boston, MA: Springer)
- [29] Wyckoff R W G 1963 *Crystal Structures* vol I (New York: Interscience)
- [30] Hulman M, Haluška M, Scalia G, Obergfell D and Roth S 2008 Effects of charge impurities and laser energy on Raman spectra of graphene *Nano Lett.* **8** 3594–7
- [31] Han W, Pi K, Bao W, McCreary K M, Li Y, Wang W H, Lau C N and Kawakami R K 2009 Electrical detection of spin precession in single layer graphene spin valves with transparent contacts *Appl. Phys. Lett.* **94** 222109
- [32] Nagashio K, Nishimura T, Kita K and Toriumi A 2010 Contact resistivity and current flow path at metal/graphene contact *Appl. Phys. Lett.* **97** 143514